

Probing nuclear compressibility via fragmentation in Au+Au reactions at 35 AMeV

Yogesh K. Vermani* and Rajiv Chugh

Department of Physics, Panjab University, Chandigarh -160 014, India

Aman D. Sood

SUBATECH - Ecole des Mines de Nantes

4, rue Alfred Kastler, F-44072 Nantes, Cedex 03, France

(Dated: September 24, 2010)

The molecular dynamics study of fragmentation in peripheral $^{197}\text{Au} + ^{197}\text{Au}$ collisions at 35 MeV/nucleon is presented to probe the nuclear matter compressibility in low density regime. The yields of different fragment species, rapidity spectra, and multiplicities of charged particles with charge $3 \leq Z \leq 80$ are analyzed at different peripheral geometries employing a soft and a hard equations of state. Fragment productions is found to be quite insensitive towards the choice of nucleon-nucleon cross sections allowing us to constrain nuclear matter compressibility. Comparison of calculated charged particle multiplicities with the experimental data indicates preference for the *soft* nature of nuclear matter.

PACS numbers: 25.70.-z 25.70.Pq 24.10.Lx

Key words: quantum molecular dynamics (QMD) model, heavy-ion collisions, multifragmentation, nuclear equation of state, Multics-Miniball array.

I. INTRODUCTION

During the last two decades, numerical simulations of medium and high energy heavy-ion (HI) reactions have provided a unique opportunity to explore the nuclear matter at the extreme conditions of density and temperature [1–5]. The compression of nuclear matter can be judged via equation of state (EoS) which is also a main input for any theoretical model along with nucleon-nucleon (n - n) cross section [4–8]. Various attempts have been made to find the observables which are sensitive to the nuclear EoS. In the past, comparison of theoretical predictions with the experimental results has been used to extract the nuclear equation of state. One of the earlier attempts for nuclear EoS (or, incompressibility) was via giant monopole resonance (GMR) studies [9, 10]. The scattering of α particles off the nucleus induces volume oscillations with $L=0$, which can be used to determine the incompressibility ' κ ' of that nucleus. These results generally yield incompressibility in the range $\kappa \sim 250$ -270 MeV indicating the matter to be softer. A recent GMR study in the ^{208}Pb and ^{90}Zn nuclei showed that the softening of nuclear matter is needed to explain the collective modes with different neutron-to-proton ratios [11]. Another study on the fusion reported linear momentum transfer to be sensitive to both the EoS and n - n cross section [12]. Within *quantum molecular dynamics* (QMD) model, an incompressibility of $\kappa=200$ MeV (*i.e.*, soft EoS) was reported to reproduce the experimental data on energy transfer in a compound nucleus formation [12].

Collective flow observed in HI collisions is another observable which is found to be sensitive towards the stiffness of nuclear EoS [6, 8, 13]. The collective transverse in-plane flow and balance energy (the energy at which flow becomes zero) have been studied extensively over the past two decades so as to constrain the EoS, but still the uncertainties are very large. For example, a stiff EoS with $\kappa=380$ MeV reproduces the transverse flow data equally well as obtained with soft momentum dependent EoS with $\kappa=210$ MeV [5, 14]. Similarly, comparison of transport model calculations with data of EOS Collaboration for the energy dependence of collective flow favored neither the 'soft' nor the 'hard' equation of state [8]. In recent comparison of elliptic flow data with microscopic transport model calculations of the Refs. [15, 16], no consistent agreement with the data could be obtained [17] for the two different models of Refs. [15] & [16]. Therefore, it is clear from the above review that an appropriate choice of the nuclear equation of state is still far from settlement. The task of deriving quantitative information about the EoS requires detailed comparison of theoretical calculations assuming different equations of state with experimental data.

*Electronic address: yugs80@gmail.com

At lower beam energies, Pauli blocking of final states gets more pronounced. As a result, mean-field effects and long range Coulomb force govern the reaction dynamics. If one goes to still lower energy regime, well-known phenomena like complete fusion, incomplete fusion, fission, cluster emission *etc.*, can be seen [18, 19]. At incident energies above 20 A MeV, phenomena like production of intermediate mass fragments (IMFs), projectile-like and target-like fragments (PLFs and TLFs) dominate the exit channel. The phenomenon of multifragment-emission in low energy domain is, however, least exploited to infer the nuclear EoS. Naturally the study of fragment-emission in low energy domain may be of importance to constrain the nuclear incompressibility, where the role of different n - n cross sections is expected to be minimal. To explore the possibility of achieving information on the nuclear EoS, we plan here to simulate the peripheral reactions of $^{197}\text{Au} + ^{197}\text{Au}$ at $E_{lab}=35$ A MeV and at different peripheral geometries where accurate data has been measured on Multics-Miniball set-up [20]. To this end, we performed detailed calculations within the *quantum molecular dynamics* (QMD) model [21, 22] which is described in detail in section II along with *simulated annealing clusterization algorithm* [23, 24]. Section III presents results of our numerical calculations and comparison with available experimental data, which are finally summarized in section IV.

II. THE MODEL

A. Quantum Molecular Dynamics (QMD) Model

The *quantum molecular dynamics* model is a n -body transport theory that incorporates the quantum features of Pauli blocking and stochastic n - n scattering. Each nucleon in the colliding system is represented by a Gaussian wave packet as:

$$\psi_i(\mathbf{r}, \mathbf{p}_i(t), \mathbf{r}_i(t)) = \frac{1}{(2\pi L)^{3/4}} \exp \left[\frac{i}{\hbar} \mathbf{p}_i(t) \cdot \mathbf{r} - \frac{(\mathbf{r} - \mathbf{r}_i(t))^2}{4L} \right]. \quad (1)$$

Mean position $\mathbf{r}_i(t)$ and mean momentum $\mathbf{p}_i(t)$ are the two time dependent parameters. The Gaussian width \sqrt{L} is fixed with a value of 1.8 fm and is same for all nucleons. This value of \sqrt{L} corresponds to a root-mean-square radius of each nucleon. The centers of these Gaussian wave packets in \mathcal{R}_3 and \mathcal{P}_3 spaces follow the trajectories according to the classical equations of motion:

$$\dot{\mathbf{p}}_i = -\frac{\partial \langle \mathcal{H} \rangle}{\partial \mathbf{r}_i}, \quad \dot{\mathbf{r}}_i = \frac{\partial \langle \mathcal{H} \rangle}{\partial \mathbf{p}_i}. \quad (2)$$

The Hamiltonian \mathcal{H} appearing in Eq. (2) has contribution from the local Skyrme-type, Yukawa and effective Coulomb interactions [21]:

$$V_{ij}^{loc} = t_1 \delta(\mathbf{r}_i - \mathbf{r}_j) + t_2 \delta(\mathbf{r}_i - \mathbf{r}_j) \delta(\mathbf{r}_i - \mathbf{r}_k) \quad (3a)$$

$$V_{ij}^{Yuk} = t_3 \frac{\exp\{-|\mathbf{r}_i - \mathbf{r}_j|/\mu\}}{|\mathbf{r}_i - \mathbf{r}_j|/\mu} \quad (3b)$$

$$V_{ij}^{Coul} = \frac{Z_i \cdot Z_j e^2}{|\mathbf{r}_i - \mathbf{r}_j|}. \quad (3c)$$

Here Z_i, Z_j are the effective charge of baryons i and j . The long-range Yukawa force is necessary to improve the surface properties of the interaction. The parameters μ, t_1, t_2, t_3 appearing in Eqs. (3) are given in Ref. [22]. These parameters are adjusted and fitted so as to achieve the correct binding energy and root mean square values of the radius of the nucleus [22]. In QMD model, one neglects the isospin dependence of nucleon-nucleon interaction. All nucleons in a nucleus are assigned the effective charge $Z = \frac{Z_T + Z_P}{A_T + A_P}$ [21]. It is worth mentioning that isospin dependent flavor of QMD model (*i.e.* IQMD) has also been used in literature [21, 25]. This microscopic transport code explicitly takes into account the differences of neutron and proton potentials and cross sections. The Skyrme part of the interaction used in QMD model has the generalized form:

$$V_{ij}^{loc} = \frac{\alpha}{2} \left(\frac{\rho_{ij}}{\rho_o} \right) + \frac{\beta}{\gamma + 1} \left(\frac{\rho_{ij}}{\rho_o} \right)^\gamma. \quad (4)$$

The interaction density in Eq. (4) is defined as:

$$\rho_{ij} = \frac{1}{(4\pi L)^{3/4}} \cdot e^{-(\mathbf{r}_i - \mathbf{r}_j)^2/4L}. \quad (5)$$

The parameters α and β are adjusted to reproduce the infinite nuclear matter binding energy ($E/A = -16$ MeV) at saturation nuclear matter density ρ_0 . The third parameter γ can be varied independently to account for different nuclear incompressibilities κ (*i.e.* different equations of state). Two different parameterizations are used: a soft EoS with incompressibility $\kappa=200$ MeV, and a hard EoS with $\kappa=380$ MeV. The parameters α , β , and γ employed in the QMD model serve as an input for repulsive potential with high compressibility (*i.e.* hard EoS), and less repulsive potential (*i.e.* soft EoS). The standard parameters corresponding to these two equations of state are listed in Table I.

TABLE I: The Skyrme parameters for ‘soft’ and ‘hard’ interactions used in the QMD model.

<i>EoS</i>	$\alpha(\text{MeV})$	$\beta(\text{MeV})$	γ	$\kappa(\text{MeV})$
Soft	-356	303	7/6	200
Hard	-124	70.5	2	380

The influence of different n - n scattering cross sections will be determined by employing a set of different cross sections varying from energy-dependent cross section [26] to constant and isotropic cross sections with magnitudes of 40 and 55 mb. It is worth mentioning that in recent times, even relativistic version has also been analyzed [1]. As noted in Ref. [1], this has no effect on present findings. A hard EoS with energy dependent cross section is labeled as *Hard^{Cg}*. Incorporation of isotropic and constant cross sections of 40 and 55 mb strengths have been labeled as *Hard⁴⁰* and *Hard⁵⁵*, respectively. Similarly, for the soft equation of state, we have *Soft^{Cg}*, *Soft⁴⁰* and *Soft⁵⁵*, respectively. Since QMD model follows the time evolution of nucleons only, one has to employ secondary clusterization algorithms to identify fragments’ structure. In the present paper, *simulated annealing clusterization algorithm* (SACA) has been used to identify final fragment structure. This method is reported to explain the ALADiN data on spectator fragmentation quite nicely at relativistic bombarding energies [24].

B. The SACA Formalism

This clusterization procedure allows early identification of fragments before these are well separated in coordinate space. In the SACA method, fragments are constructed based on the energy correlations. It works on the principle of energy minimization of fragmenting system. Standard *minimum spanning tree* (MST) procedure [22] is employed to obtain pre-clusters. This procedure assumes that nucleon pairs separated by distance $|\mathbf{r}_i - \mathbf{r}_j| \leq 4$ fm, belong to the same fragment [6, 22]. Such preliminary cluster configuration is determined at every time step. Thus one can address the time evolution of mass, charge, position and momentum of each fragment or single nucleon. The pre-clusters obtained with the MST method [22, 27] are subjected to a binding energy check [23]:

$$\zeta_i = \frac{1}{N_f} \sum_{\alpha=1}^{N_f} \left[\sqrt{(\mathbf{p}_\alpha - \mathbf{P}_{N_f^{c.m.}})^2 + m_\alpha^2} - m_\alpha + \frac{1}{2} \sum_{\beta \neq \alpha}^{N_f} V_{\alpha\beta}(\mathbf{r}_\alpha, \mathbf{r}_\beta) \right] < -E_{bind}, \quad (6)$$

with $E_{bind} = 4.0$ MeV if $N_f \geq 3$ and $E_{bind} = 0$ otherwise. In Eq. (6), N_f is the number of nucleons in a fragment and $\mathbf{P}_{N_f^{c.m.}}$ is the center-of-mass momentum of the fragment. The requirement of a minimum binding energy excludes the loosely bound fragments which will decay at later stage. To look for the most bound configuration (MBC), we start from a random configuration which is chosen by dividing whole system into few fragments. The energy of each cluster is calculated by summing over all the nucleons present in that cluster using Eq. (6).

Let the total energy of a configuration k be $E_k (= \sum_i N_f \zeta_i)$, where N_f is the number of nucleons in a fragment and ζ_i is the energy per nucleon of that fragment. Suppose a new configuration k' (which is obtained by (a) transferring a nucleon from randomly chosen fragment to another fragment or by (b) setting a nucleon free, or by (c) absorbing a free nucleon into a fragment) has a total energy $E_{k'}$. If the difference between the old and new configuration $\Delta E (= E_{k'} - E_k)$ is negative, the new configuration is always accepted. If not, the new configuration k' may nevertheless be accepted with a probability of $\exp(-\Delta E/v)$, where v is called the control parameter. This procedure is known as Metropolis algorithm. The control parameter is decreased in small steps. This algorithm will yield eventually the most bound configuration (MBC). Since this combination of a Metropolis algorithm with slowly decreasing control parameter v is known as *simulated annealing*, so our approach is dubbed as *simulated annealing clusterization algorithm* (SACA). We have used here an extended version of SACA, in which each cluster is subjected to its true binding energy based upon modified Bethe-Weizsäcker mass formula [28]. It may be stated that fragmentation analysis performed within extended version yields the same results as with constant binding energy check of -4 MeV/nucleon. It also

justifies using extended approach to analyze the fragmentation at such a low incident energy when nuclei are still in Fermi energy domain. The constant binding energy criterion (of -4 MeV/nucleon) is chosen keeping in mind the average binding energy of clusters. We have also analyzed the fragmentation pattern employing E_{bind} based upon experimental binding energies. Nearly no effect of this modification was found. For further details, we refer the reader to Refs. [23, 24, 27, 28].

III. RESULTS AND DISCUSSION

Figure 1 shows the time evolution of $^{197}\text{Au} + ^{197}\text{Au}$ reaction at 35 AMeV with reduced impact parameters $b/b_{max}=0.55$ (left panel) and 0.85 (right panel). Top panel depicts the time evolution of average nucleon density ρ^{avg} for soft and hard EoS. One notices several interesting results: (i) Maximal density is reached nearly at the same time at both impact parameters, whereas saturated values is slightly more for higher impact parameters, (ii) Choice of different n - n cross sections have insignificant influence on the results obtained. This happens due to effective Pauli blocking at such a low incident energy that prohibits n - n collisions.

Stiffness of nuclear EoS, however significantly influences the mean nucleon density ρ^{avg} and other fragment observables shown in subsequent windows. This difference is clearly visible in the evolution of heaviest fragment $\langle A^{max} \rangle$, multiplicities of free particles, light charged particles LCPs [$2 \leq A \leq 4$], and clusters with mass $A \geq 5$. The mean size of heaviest fragment $\langle A^{max} \rangle$ attains minimum around 100 fm/c, where stable fragment configuration can be realized and compared with experimental results. With stiff EoS, heavier $\langle A^{max} \rangle$ is registered. Interestingly, multiplicity of free particles obtained also follows the same trend as $\langle A^{max} \rangle$. This means that dissipation of energy takes place mainly via emission of free-nucleons that cools down the nuclear system in case of hard EoS. Consequently, lesser yields of LCPs and fragments with mass $A \geq 5$ are obtained with a stiff EoS. On other hand, soft EoS favors emission of LCPs and heavier fragments ($A \geq 5$) from spectator zone, thereby decreasing the size of A^{max} . The insensitivity of fragmentation pattern towards choice of different n - n cross sections may be, therefore, useful to constrain the nuclear compressibility in low density regime.

Next we study the rapidity spectra of free nucleons and intermediate mass fragments in transverse and longitudinal direction using a hard and a soft equations of state. The transfer of excitation energy from the participant zone to spectator matter has a direct bearing on the rapidity distribution of the fragments. Figure 2 displays the spectrum of scaled transverse $y^{(x)}$ and longitudinal $y^{(z)}$ rapidity distribution of free particles (top) and intermediate mass fragments IMFs [$5 \leq A \leq 65$] (bottom) for the collision of Au (35 AMeV)+ Au at reduced impact parameter $b/b_{max}=0.55$. As expected, the rapidity spectrum of free nucleons and IMFs is quite sensitive to the nuclear EoS that brings out significant change in their transverse expansion as well as stopping pattern. Using hard interactions, a larger fraction of free nucleons are emitted into transverse direction. IMFs aren't, however, dispersed much into transverse directions and continue to move at target and projectile velocities. Similar trends are visible for longitudinal rapidity (y_z) distribution as well. Using a 'stiff' EoS, system seems to cool-off via abundant production of the free nucleons from the midrapidity as well as from the spectator zone, whereas a 'soft' EoS contributes significantly towards the IMFs emission at target and projectile rapidities. It means that system propagating under the soft interactions is less equilibrated. As a result, heavier fragments leave the participant zone quite early and suffer less collisions. These findings suggest that fragment emission from the decay of spectator component is quite sensitive to the mean field and compressibility of participant matter.

Finally we calculate the multiplicity of charged particles with $3 \leq Z \leq 80$ using a hard and a soft equations of state for Au(35 AMeV)+Au collisions at six peripheral geometries (see Fig. 3). The multiplicities calculated at 100 fm/c are subjected to forward rapidity condition ($y > 0.5 y_{beam}$) in the center-of-mass frame to exclude events from midrapidity and quasitarget decay. Also shown in the figure is integrated multiplicities of charged particles with charge $3 \leq Z \leq 80$ (i.e. $\int_3^{80} N(Z)dZ$) obtained on Multics-Miniball setup [20]. It is worth mentioning that multiplicities were calculated keeping in mind the angular range covered by combined Multics-Miniball array. Overall we can see that results obtained with a *soft* EoS are consistent with experimental data at all colliding geometries. These findings reflects the ability of molecular dynamics approaches (QMD, in our case) to describe the reaction dynamics in low-energy regime.

Due to more explosive nature of hard EoS, spectator matter mainly de-excites via emission of free nucleons and therefore, decline in multiplicity of heavier clusters occurs. An increasing trend of fragment multiplicity with centrality can be understood in terms of more excitation energy deposited in spectator matter. In semi-peripheral events, a larger chunk of excitation energy gets transferred to spectator matter, thereby, leading to rise in multiplicity of fragments with decrease in impact parameter. Nuclear mean-field, therefore, becomes important factor governing the outcome of spectator decay, while nucleon-nucleon collisions dominate the participant matter physics. This analysis clearly illustrates the relatively *soft* nature of nuclear matter.

IV. SUMMARY

In summary, QMD model has been used to infer the inter-play of different model inputs on fragment-emission in peripheral $^{197}\text{Au} + ^{197}\text{Au}$ collisions at 35 AMeV. We find that choice of different nucleon-nucleon cross sections has marginal role to play at such a low incident energy. However, the multiplicity of charged particles obtained from the spectator decay are strongly influenced by the incompressibility of the nuclear matter. The hard equation of state results in enhanced emission of free nucleons and fewer heavier fragments. Model calculations with soft EoS are found to give encouraging results which are in accord with experimental trends. This study favors *soft* nature of the nuclear matter.

V. ACKNOWLEDGEMENTS

One of the authors (Y. K. V) is acknowledges constructive discussions with Drs. M. D' Agostino and M. Bruno. The research grant from Indo-French Center for the Promotion of Advanced Research (IFCPAR), New Delhi vide grant no. IFC/4104-1 is gratefully acknowledged.

-
- [1] R. K. Puri *et al.*, Nucl. Phys. A **575**, 733 (1994); E. Lehmann, R. K. Puri, A. Faessler, G. Batko and S. W. Huang, Phys. Rev. C **51**, 2113 (1995); E. Lehmann *et al.*, Prog. Part. Nucl. Phys. **30**, 219 (1993); S. W. Huang *et al.*, Phys. Lett. B **298**, 41 (1993).
 - [2] A. Bohnet, N. Ohtsuka, J. Aichelin, R. Linden and A. Faessler, Nucl. Phys. A **494**, 349 (1989); D. T. Khoa *et al.*, Nucl. Phys. A **542**, 671 (1992); G. Q. Li *et al.*, Z. Phys. A **340**, 271 (1991); D. T. Khoa *et al.*, Nucl. Phys. A **548**, 102 (1992).
 - [3] C. Fuchs, E. Lehmann, R. K. Puri, L. Sehn, A. Faessler and H. H. Wolter, J. Phys. G: Nucl. Part. Phys. **22**, 131 (1996); S. Kumar, R. K. Puri and J. Aichelin, Phys. Rev. C **58**, 1618 (1998); Y. K. Vermani, S. Goyal and R. K. Puri, Phys. Rev. C **79**, 064613 (2009).
 - [4] A. D. Sood and R. K. Puri, Phys. Rev. C **70**, 034611 (2004); S. Kumar, S. Kumar and R. K. Puri, Phys. Rev. C **78**, 064602 (2008); Y. K. Vermani and R. K. Puri, J. Phys. G: Nucl. Part. Phys. **36**, 105103 (2009).
 - [5] J. Aichelin, A. Rosenhauer, G. Peilert, H. Stöcker and W. Greiner, Phys. Rev. Lett. **58**, 1926 (1987); C. Gale, G. F. Bertsch and S. Das Gupta, Phys. Rev. C **35**, 1666 (1987).
 - [6] G. Peilert *et al.*, Phys. Rev. C **39**, 1402 (1989); Mod. Phys. Lett. A **3**, 459 (1988).
 - [7] M. Berenguer *et al.*, J. Phys. G: Nucl. Part. Phys. **18**, 655 (1992).
 - [8] M. D. Partlan *et al.*, Phys. Rev. Lett. **75**, 2100 (1995).
 - [9] D. H. Youngblood, H. L. Clark and Y. W. Lui, Phys. Rev. Lett. **82**, 691 (1999); J. Piekarewicz, Phys. Rev. C **69**, 041301(R) (2004), and references therein.
 - [10] M. Itoh *et al.*, Nucl. Phys. A **687**, 52 (2001).
 - [11] B. G. Todd-Rutel and J. Piekarewicz, Phys. Rev. Lett. **95**, 122501 (2005).
 - [12] J. Cibor, J. Lukasik and Z. Majka, Z. Phys. A **348**, 233 (1994); F. Haddad *et al.*, Phys. Rev. C **53**, 1437 (1996).
 - [13] D. J. Magestro, W. Bauer and G. D. Westfall, Phys. Rev. C **62**, 041603(R) (2000).
 - [14] Q. Pan and P. Danielewicz, Phys. Rev. Lett. **70**, 2062 (1993).
 - [15] A. B. Larionov, W. Cassing, C. Greiner and U. Mosel, Phys. Rev. C **62**, 064611 (2000).
 - [16] P. Danielewicz, R. Lacey and W. G. Lynch, Science **298**, 1592 (2002).
 - [17] A. Andronic *et al.*, Phys. Lett. B **612**, 173 (2005).
 - [18] R. K. Puri, P. Chattopadhyay and R. K. Gupta, Phys. Rev. C **43** (1991) 315; R. K. Puri and R. K. Gupta, Phys. Rev. C **45**, 1837 (1992); J. Phys. G: Nucl. Part. Phys. **18**, 903 (1992); R. K. Gupta, S. Singh, R. K. Puri and W. Scheid, Phys. Rev. C **47**, 561 (1993); S. S. Malik *et al.*, Pramana J. Phys. **32**, 419 (1989); R. K. Puri, S. S. Malik and R. K. Gupta, Europhys. Lett. **9**, 767 (1989); R. Arora, R. K. Puri and R. K. Gupta, Eur. Phys. J. A **8**, 103 (2000); R. K. Puri and N. K. Dhiman, Eur. Phys. J. A **23**, 429 (2005); R. K. Gupta, M. Balasubramaniam, R. K. Puri and W. Scheid, J. Phys. G: Nucl. Part. Phys. **26**, L23 (2000).
 - [19] R. K. Gupta *et al.*, J. Phys. G: Nucl. Part. Phys. **18**, 1533 (1992); I. Dutt and R. K. Puri, Phys. Rev. C **81**, 047601 (2010); Phys. Rev. C **81**, 044615 (2010); Phys. Rev. C **81**, 064609 (2010); Phys. Rev. C **81**, 064608 (2010).
 - [20] M. D'Agostino *et al.*, Nucl. Phys. A **650**, 329 (1999).
 - [21] Ch. Hartnack *et al.*, Eur. Phys. J. A **1**, 151 (1998); A. D. Sood and R. K. Puri, Phys. Rev. C **79**, 064618 (2009).
 - [22] J. Aichelin, Phys. Rep. **202**, 233 (1991).
 - [23] P. B. Gossiaux, R. K. Puri, Ch. Hartnack and J. Aichelin, Nucl. Phys. A **619**, 379 (1997); R. K. Puri and J. Aichelin, J. Comput. Phys. **162**, 245 (2000).
 - [24] Y. K. Vermani and R. K. Puri, Europhys. Lett. **85**, 62001 (2009).

- [25] S. Gautam, R. Chugh, A. D. Sood, R. K. Puri, Ch. Hartnack and J. Aichelin, J. Phys. G: Nucl. Part. Phys. **37**, 085102 (2010); S. Kumar, S. Kumar and R. K. Puri, Phys. Rev. C **81**, 014601; Phys. Rev. C **81**, 014611 (2010).
- [26] J. Cugnon, T. Mizutani and J. Vandermeulen, Nucl. Phys. A **352**, 505 (1981).
- [27] J. Singh and R. K. Puri, J. Phys. G: Nucl. Part. Phys. **27**, 2091 (2001).
- [28] Y. K. Vermani, J. K. Dhawan, S. Goyal, R. K. Puri and J. Aichelin, J. Phys. G: Nucl. Part. Phys. **37**, 015105 (2010).

Figure Captions

FIG. 1. QMD simulation of Au (35 AMeV)+Au collisions at reduced impact parameter $b/b_{max}=0.55$ (left panel) and $b/b_{max}=0.85$ (right panel) as a function of time: (a) mean nucleon density ρ^{avg}/ρ_o ; (b) size of heaviest fragment A^{max} ; multiplicities of (c) free nucleons, (d) light charged particles LCPs, and (e) fragments with mass $A \geq 5$, respectively.

FIG. 2. Rapidity distribution dN/dy of free nucleons and intermediate mass fragments (IMFS) as a function of scaled transverse, $y^{(x)}/y_{beam}$ (left) and longitudinal, $y^{(z)}/y_{beam}$ (right) rapidities in Au (35 AMeV)+Au reaction at reduced impact parameter $b/b_{max}=0.55$. Solid and dashed curves correspond to model calculations using a ‘soft’ and a ‘hard’ EoS respectively.

FIG. 3. The impact parameter dependence of multiplicity of fragments with charge $3 \leq Z \leq 80$ obtained using a ‘soft’ EoS (solid line) and a ‘hard’ EoS (dashed line) in Au(35 AMeV)+Au collisions. Filled circles depict the experimental data points [20].

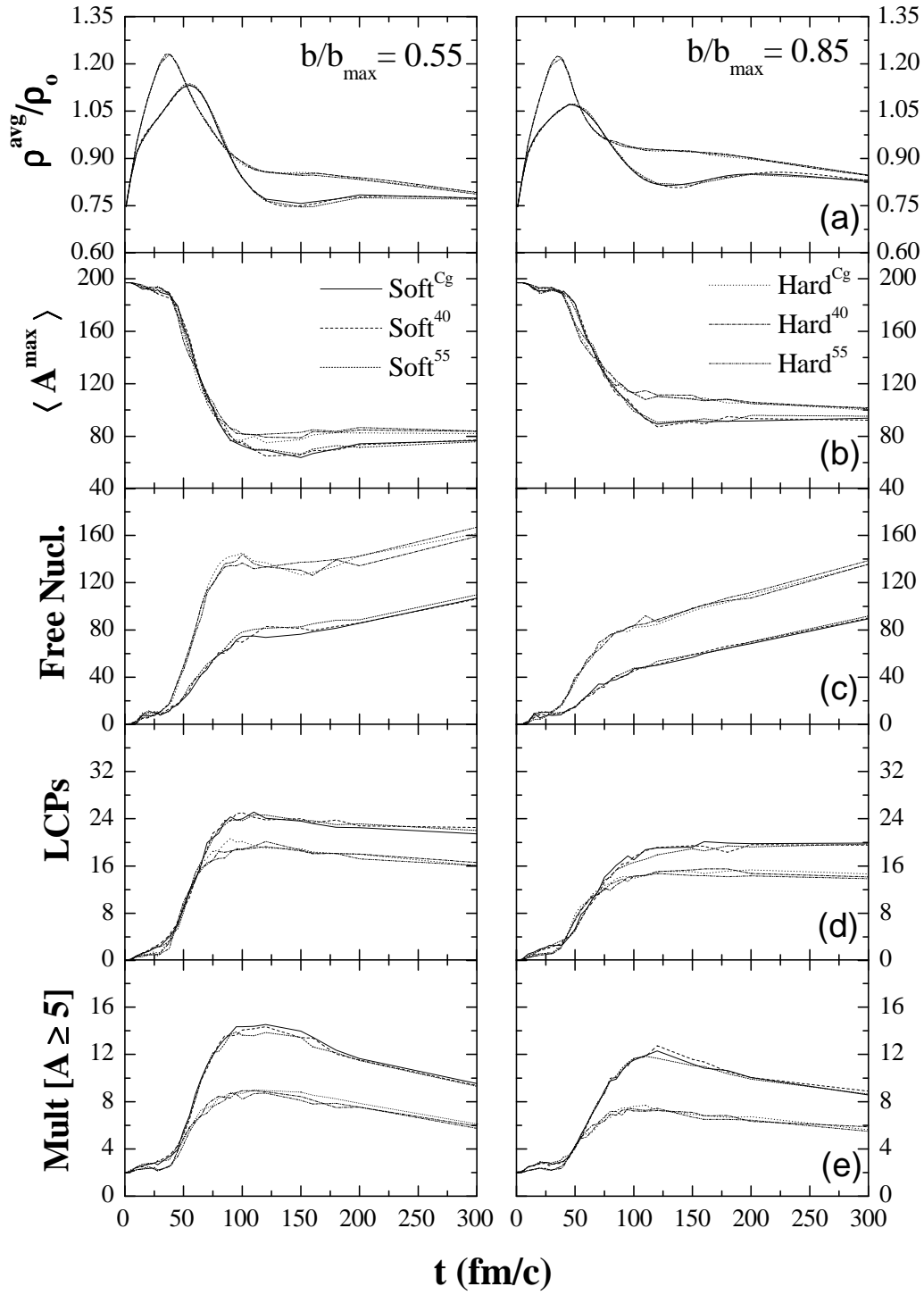


FIG. 1:

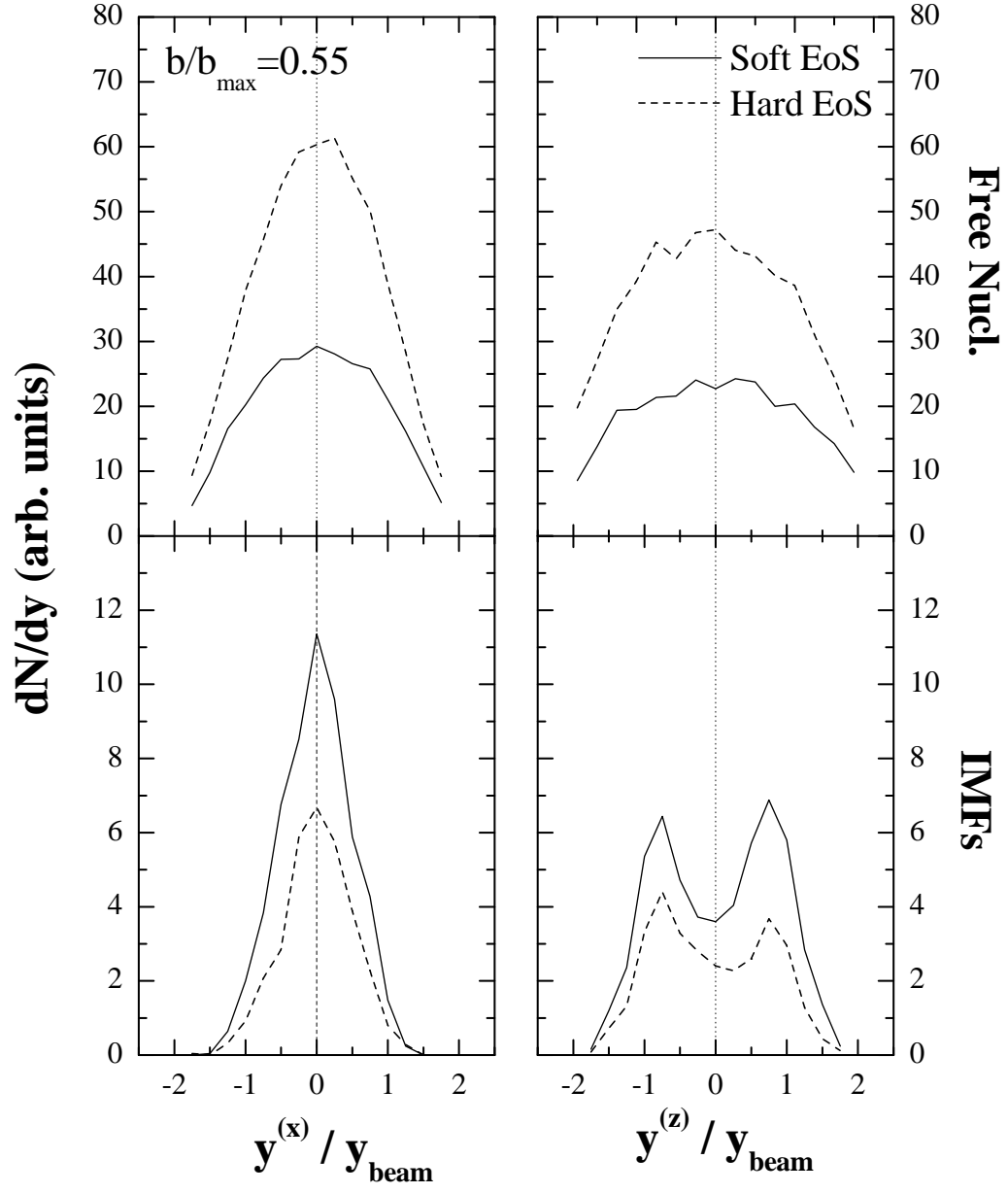


FIG. 2:

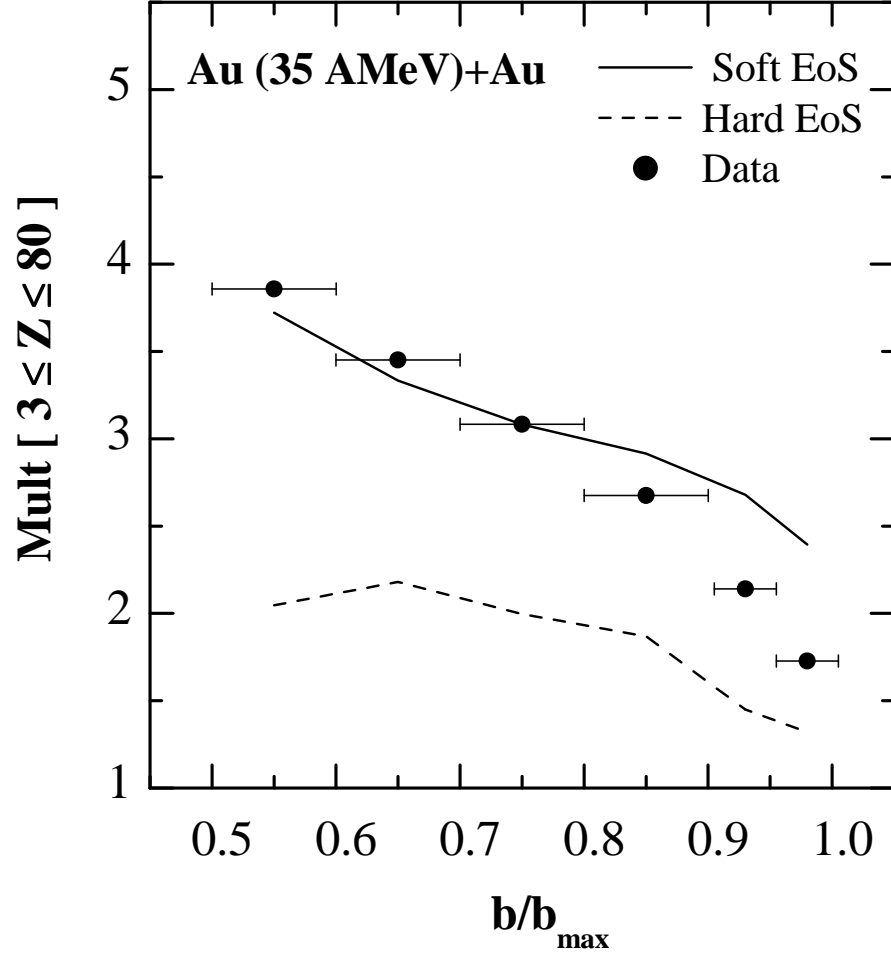


FIG. 3: